Supporting Information

Low-cost dopant-free carbazole enamine hole-transporting materials for thermally stable perovskite solar cells.

Suer Zhou[a], Maryte Daskeviciene[b], Matas Steponaitis[b], Giedre Bubniene[b], Vygintas Jankauskas[c], Kelly Schutt[a], Philippe Holzhey[a], Ashley Marshall[a], Pietro Caprioglio[a], Grey Christoforo[a], James M. Ball[a], Tadas Malinauskas[b], Vytautas Getautis[b] and Henry J. Snaith[a]*.*

[a] Department of Physics Clarendon Laboratory, University of Oxford Parks Road, Oxford, OX1 3PU, UK

[b] Department of Organic Chemistry, Kaunas University of Technology, Radvilenu pl. 19, LT-50254, Kaunas, Lithuania

[c] Institute of Chemical Physics, Vilnius University, Sauletekio av. 9, LT- 10222, Vilnius, Lithuania

*Corresponding authors: vytautas.getautis@ktu.lt, henry.snaith@physics.ox.ac.uk

Experimental Details and Methods

Materials

Tin (IV) oxide (SnO_2, 15% in H_2O colloidal dispersion) was purchased from Alfa Aesar. Formamidinium iodide (FAI) (>99.99%) was purchased from Greatcell Solar Materials, and cesium iodide (CsI) (>99.999%) was purchased from Alfa Aesar. PbI_2 and $PbBr_2$ were purchased from TCI. Spiro-OMeTAD (>99.5%) was obtained from Lumtech. Lithium bis(trifluoromethanesulfonyl)imide (Li-TFSI, >99%), 4-tert-butylpyridine (tBP, 98%), Isopropanol (IPA, 99.5%), N, N-dimethylformamide (DMF, anhydrous 99.8%), dimethyl sulfoxide (anhydrous DMSO, >99.9%), anisole (anhydrous, 99.7%), chlorobenzene (CB, 99.8%), acetonitrile (ACN, anhydrous 99.8%) were purchased from Sigma Aldrich. PCBM (99.5%) was purchased from Ossila. Gold pellets for evaporation was purchased from Kurt J. Lesker. Chemicals were purchased from Sigma-Aldrich and TCI Europe and used as received without further purification. The course of the reactions were monitored by TLC (thin layer chromatography) on ALUGRAM SIL G/UV254 plates and developed with UV light. Silica gel (grade 9385, 230–400 mesh, 60 Å, Aldrich) was used for column chromatography. The 1H and 13C NMR spectra were taken on Bruker Avance III 400 (400 MHz) and Bruker Avance III 700 (700 MHz) spectrometers at room temperature. The chemical shifts, expressed in δ (ppm) are relative to a (CH3)4Si (TMS, 0 ppm) internal standard. Elemental analysis was performed with an Exeter Analytical CE-440 elemental analyzer, Model 440 C/H/N/. MS spectroscopy was done using Waters HPLC-system with UV (200-700 nm) and MS (20-2000 m/z) detectors. Thermogravimetric analysis (TGA) was performed on a Q50 thermogravimetric analyzer (TA Instruments) at a scan rate of 10 K min^{-1} in a nitrogen atmosphere. Differential scanning calorimetry (DSC) was performed on a Q10 calorimeter (TA Instruments) at a heating rate of 10 K/min in a nitrogen atmosphere. The glass transition temperatures for the investigated compounds were determined during the second heating scan. Melting point for crystalline materials were observed using Mel-Temp DigiMelt MPA 161 melting point apparatus at a heating rate of 1 C°/min.

Optical measurements

Absorption spectra of the synthesized enamines were measured in dilute solutions in THF (concentration 10^{-4} M) and on glass substrate using a UV/Vis–NIR spectrophotometer, Lambda 35 (Perkin–Elmer).

Steady-State and Time-Resolved Photoluminescence

Time-resolved PL measurements were acquired using a time-correlated single-photon counting (TCSPC) setup (FluoTime 300, PicoQuant GmbH). Film samples were photoexcited using a 510 nm laser head (LDH-P-C-510, Pico Quant GmbH) pulsed at frequency of 1 MHz, with a pulse duration of 1 ns and fluence of 30 nJ/cm^{-2}. The PL was collected using a high-resolution monochromator and hybrid photomultiplier detector assembly (PMA Hybrid 40, PicoQuant GmbH). The laser was illuminated from the glass side. The time-resolved PL decays were fitted to a stretched exponential function

$$f(t) = A \cdot exp(-\frac{t}{\tau})^{\beta} \qquad \text{Equation (S1).}$$

in which β is the stretching parameter. $0<\beta<1$ indicates how much the curve deviates from a mono-exponential decay of $\beta=1$. The mean lifetime of the photogenerated charges $\langle\tau\rangle$ is given by

$$\langle\tau\rangle = \int_0^{\infty} dt\ exp(-(\frac{t}{\tau})^{\beta}) = \frac{\tau}{\beta}\ \mathbf{\Gamma(\frac{1}{\beta})} \qquad \text{Equation (S2).}$$

where Γ is the gamma function. The fitting method is detailed in this paper published by Habisreutinger et al.[1]

Photoluminescence Quantum Efficiency (PLQE)

PLQE values were determined following the method of De Mello et al.[2] using a 532 nm continuous wave laser excitation source (Roithner, RLTMLL-532 2 W) to illuminate a sample in an integrating sphere (Newport, 70682NS), and the laser scatter and PL were collected using a fiber-coupled spectrometer (Ocean Optics MayaPro). The beam intensity was modified using neutral density filters. The laser was illuminated from the glass side for both the perovskite/HTM films and the full devices.

The quasi-Fermi level splitting (QFLS) analysis was done using methods previously reported by Caprioglio et al[3,4]. with slight modifications. To obtain PLQE values that correlate with a device operating under 1 sun illumination, an optical density filter which results in a power density of 56 mW/cm^2 was used. For a 532nm laser measuring a 1.6eV bandgap perovskite ($FA_{0.83}Cs_{0.17}Pb(I_{0.9}Br_{0.1})_3$ used in this study), this power density is equivalent to the corresponding PV device steady-state absorbed photon flux under AM 1.5. See Kirchartz et al, [5] Figure 3.

Ionization-potential measurements (I_p)

The ionization potential (I_p) of each enamine compound was measured by electron photoemission in air (the error of this method is evaluated as ±0.03eV). The samples were prepared by dissolution in THF and the solutions were coated on Al plates pre-coated with a methyl methacrylate and methacrylic acid copolymer adhesive layer (~0.5 mm). The thickness of the transporting material layer was 0.5 – 1 mm. The organic materials investigated are stable enough to oxygen that the measurements may be carried out in ambient conditions. The samples were illuminated with monochromatic light from a quartz monochromator fitted with a deuterium lamp. The power of the incident light beam was $(2–5)\cdot10^{-8}$ W. A negative voltage (-330 V) was supplied to the sample substrate. The counter electrode with a 4.5mm × 15 mm slit for illumination was placed 8 mm from the sample surface. The counter electrode was connected to the input of the BK2–16 type electrometer, working in the open input regime, for the photocurrent measurement. The $10^{-15} – 10^{-12}$ A photocurrent (I) flowed in the circuit under illumination. The value of I is strongly dependent on the incident-light photon energy (hv). The dependence $I^{0.5}$ on incident-light quanta energy hν was plotted from the experiment results. Usually, the dependence of I on the incident light quantum energy is described well by the linear relationship $I^{0.5} = f(hv)$ near the threshold. The linear part of this dependence was extrapolated to the hv axis and the I_p value was determined as the photon energy at the interception point.

Contact Angle Measurement

The contact angles of the HTM films were measured using a video-based optical contact angle measuring device (Ossila Contact Angle Goniometer) and analyzed using the Ossila Contact Angle 3.0.9.1 software. All measurements were performed in ambient atmosphere and at room temperature.

Device Fabrication

Substrate preparation. Fluorine-doped tin oxide (FTO) on glass substrates (TEC 7, sheet resistance 7~8 ohms per square) were etched with zinc powder with 2 M hydrochloric acid (HCl) to produce device patterns. The substrates were cut into 30×30 mm square pieces. The substrates were subsequently sonicate-cleaned with a 1 vol% (in D.I. water) solution of Decon 90 cleaning agent, then deionized water, acetone, and isopropanol for 10 minutes each. The

substrates were dried with a dry nitrogen stream. Then the substrates were treated with oxygen-plasma cleaning for 15 minutes before use.

Preparation of FACs on SnO_x

Tin oxide electron transport layer. SnOx nanocrystals in H_2O 15 wt% colloidal dispersion was diluted to 2 % wt% in de-ionized water. The solution was spin-coated in ambient conditions onto FTO/glass at a spin rate of 4,000 rpm for 30 sec. Substrates were annealed at 180°C for 30 min. Before spinning the perovskite layer, the substrates were treated with UV-ozone for 10 minutes.

PCBM Passivation on SnO_x for Devices for Stability Studies

The devices used for stability testing had an extra layer of PCBM in between the SnO_x and perovskite. The PCBM solution was prepared by dissolving 5 mg/mL of PCBM in chlorobenzene and stirred at room temperature overnight. The solution was filtered through a 0.22 μm filter before use. The solution was dynamically spin-coated on the substrate at 2,000 rpm, 2,000 rpm/sec acceleration for 30 seconds in a nitrogen-purged drybox with <10% relative humidity. Then the substrates were dried on a hot plate at 100 °C for 10 minutes.

FACs perovskite layer

1.45 M $FA_{0.83}Cs_{0.17}Pb(I_{0.9}Br_{0.1})_3$ precursor solution was made by dissolving 64 mg CsI, 80 mg $PbBr_2$, 207 mg FAI, and 568 mg PbI_2 into 1 mL of a DMF:DMSO solvent mixture (4:1 volume ratio). The precursor solution was heated and stirred on a hotplate at 70°C for 15 minutes under nitrogen atmosphere before use. The solution was cooled to room temperature and transferred to a nitrogen-purged drybox at around 10% relative humidity for perovskite deposition. Then 35 μL of the precursor solution was spread on an FTO/SnO_2 substrate using a pipette tip and then spun at a spin speed of 6,000 rpm for 35 sec (with a ramp speed of 2000 rpm/sec). 100 μL anisole was dropped at the center 10 sec before the end of spinning. The perovskite layers were annealed on a hotplate at 100 °C for 15 min.

Hole transport layer and electrode deposition

The hole transport material (HTM) 2,2',7,7'-tetrakis(N,N'-di-p-methoxyphenylamine)-9,9'-spirobifluorene (spiro-OMeTAD) was prepared by dissolving 85mg of spiro-OMeTAD in 1 mL anhydrous chlorobenzene along with 20μL Li-TFSI solution (500mg/mL in acetonitrile) and 33μL tBP. 50μL of spiro-OMeTAD solution was dynamically spin-coated at 2500 rpm for 30 sec.

MeO5PECz solution was prepared by dissolving 25 mg MeO5PECz in 1 mL anhydrous chlorobenzene along with 20 μL Li-TFSI solution (64.6 mg/mL) to achieve 25 mol% Li-TFSI with respect to MeO5PECz (Mw=1388.67 g/mL). 33 μL tBP was added to the solution. The solution was stirred and heated at ~60 °C overnight until the solvents had completely dissolved. Then the solution was passed through a 0.22 μL polytetrafluoroethylene (PTFE) syringe filter. 50 μL of MeO5PECz solution was dynamically deposited onto the samples at 2,500 rpm for 30 sec. The dopant-free MeO5PECz solution and the tBP dopant-only solution were prepared in a similar way.

MeO4PEBCz solution was prepared by dissolving 25 mg MeO4PEBCz in 1 mL anhydrous chlorobenzene along with 20 μL Li-TFSI solution (74.4 mg/mL) to achieve 25 mol% Li-TFSI with respect to MeO4PEBCz (Mw=1206.49 g/mol). 33 μL tBP was added to the solution. The solution was stirred and heated at ~60 °C overnight until the solvents had completely dissolved. Then the solution was passed through a 0.22 μL polytetrafluoroethylene (PTFE) syringe filter. 50 μL of MeO4PEBCz solution was dynamically deposited onto the samples at 2,500 rpm for 30 sec. The dopant-free MeO4PEBCz solution and the tBP dopant-only solution were prepared in a similar way.

The devices with HTM that contained Li-TFSI were left in a desiccator box for 24 hours for the HTMs to oxidize. Meanwhile, the devices that did not contain Li-TFSI were left in a glovebox with an inert atmosphere of N_2. Afterward, 75 nm gold electrodes were evaporated onto the samples under vacuum of $<7\times10^{-6}$ Torr.

Solar cell characterization

The photovoltaic devices were characterized in ambient condition with the room temperature around 20~24 °C and 45% relative humidity under AM1.5G simulated sunlight generated by a class AAA WaveLabs Sinus-220 solar simulator, using a Keithley 2400 source meter. The intensity of the solar simulator was set to produce 100 mW/cm^2 equivalent irradiance using a certified KG3-filtered Si reference photodiode (Fraunhofer ISE). The voltage was swept at a rate of 0.61 V/s first from forward bias to reverse bias (forward sweep) followed by a reverse sweep in the opposite scan direction. The minimum voltage was -0.1V and the maximum voltage was 1.2V. On each substrate, there were 3 devices with an area 0.25 cm^2 and 1 larger

device with an area of 1.00 cm^2. The areas were defined using black anodized aluminum shadow masks in direct contact with the glass side of the substrates within enclosed sample holders.

Device Stability Measurements

The 85 °C thermal aging test was done on unencapsulated devices in a dark nitrogen atmosphere. Devices were put inside a home-built oven with temperature control set to 85 °C (±3 °C) and removed periodically to measure device performance under ambient conditions.

The 85 °C light aging test was done on encapsulated devices in ambient atmosphere, 85 °C, full spectrum pulsed light ATLAS SUNTEST XLS+ aging box. The (1,700 W) xenon lamp is pulsed at 100 Hz and averaged off to 1 sun intensity.

The cross-sectional SEM images of the 85 °C nitrogen aged devices were taken using a Hitachi S-4300 SEM at an accelerating voltage of 10 kV.

Additional Information

Thermal properties

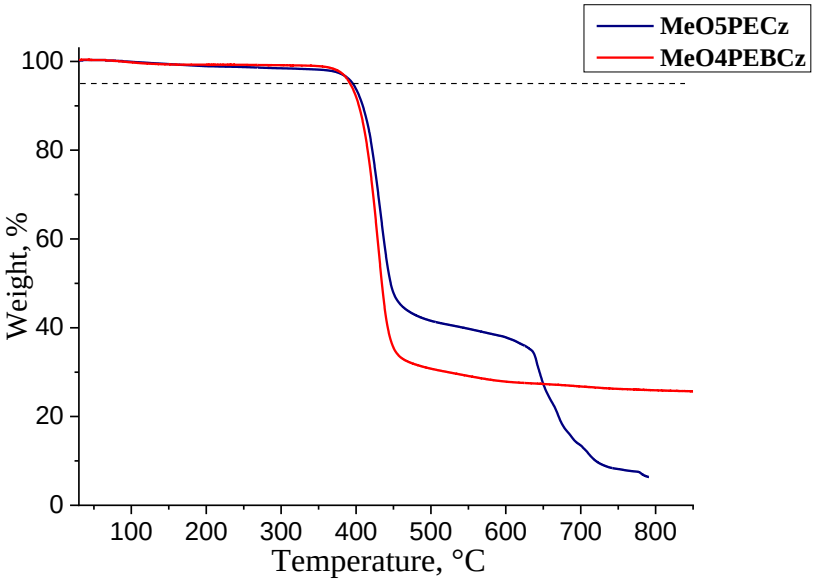

S 1.TGA heating curves of MeO5PECz and MeO4PEBCz.

Table S1. Thermal characteristics of the new HTMs and spiro-OMeTAD for comparison.

Compound	T_g [a], °C	T_m [b], °C	T_{cr} [c], °C	$T_{5\%}$ [d], °C
MeO5PECz	152	204	-	395
MeO4PEBCz	140	260	214	392
Spiro-OMeTAD	126	245	-	449

[a)]Determined by DSC: scan rate = 10 °C min^{-1}, N_2 atmosphere; second run;
[b)]Determined by DSC: scan rate = 10 °C min^{-1}, N_2 atmosphere; first run;
[c)]Determined by DSC: scan rate = 10 °C min^{-1}, N_2 atmosphere;
[d)]5% weight loss determined by TGA: heating rate = 10 °C min^{-1}, N_2 atmosphere.

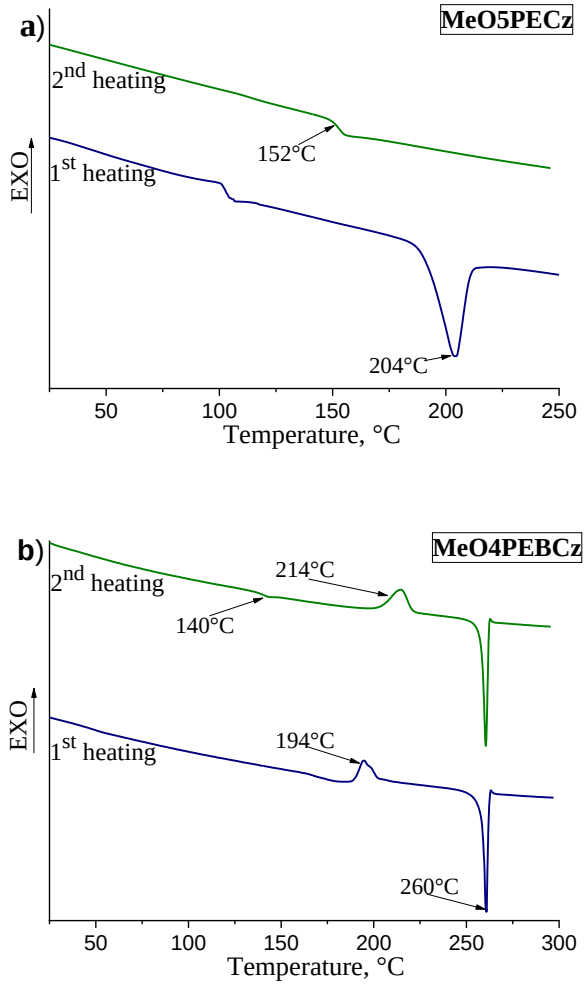

S 2. DSC heating curves of a) MeO5PECz and b) MeO4PEBCz (heating and cooling rate 10 K min^{-1}).

Optical and Photoelectrical properties

The ultraviolet-visible (UV-vis) absorption spectra of the investigated carbazole derivatives were recorded in THF solutions and on glass substrates. The additional bis(4-methoxyphenyl)ethenyl moiety in MeO5PECz does not increase the size of the π-conjugated system very significantly and only a small bathochromic shift (3-5nm) is observed, thus the absorption spectra are very similar for both compounds (Figure 3).

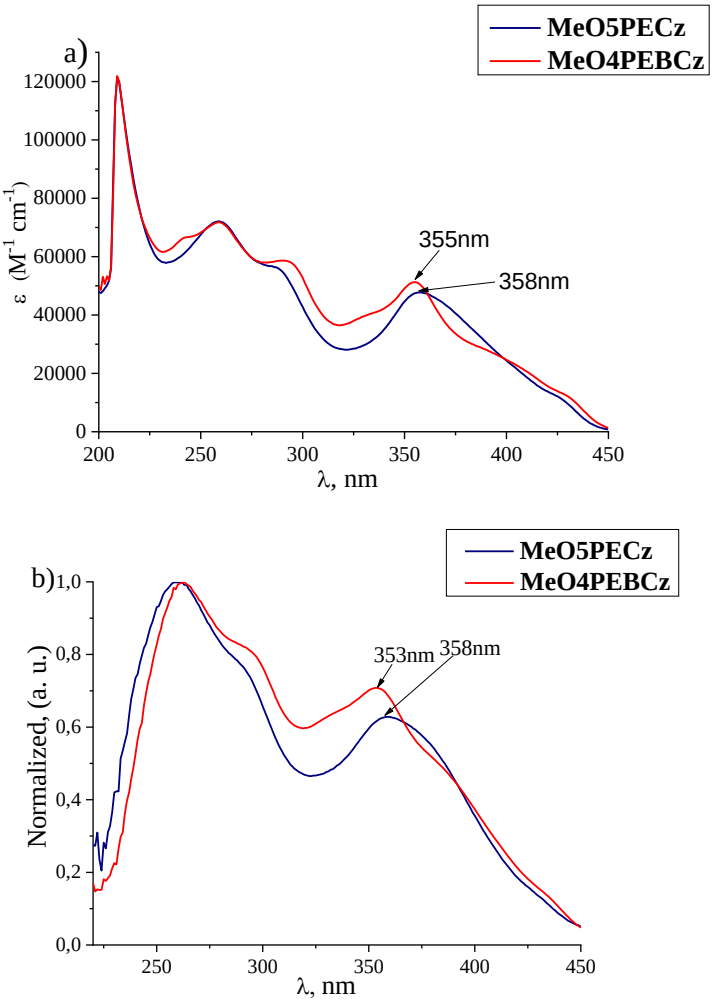

S 3. a) UV-vis absorption spectra of carbazole derivatives MeO5PECz, MeO4PEBCz in THF (conc. 1×10^{-4} M) and b) thin-films on glass.

Charge carrier mobility measurements (μ)

The samples for the charge carrier mobility measurements were prepared by spin coating solutions of the synthesized compounds in THF onto polystyrene films with a conductive Al

layer. The layer thickness was in the range 5 – 10 μm. The charge drift mobility was measured by Xerographic time of flight (XTOF). An electric field was created by positive corona charging. The charge carriers were generated at the layer surface by illumination with pulses of a nitrogen laser (pulse duration = 2 ns, λ = 337 nm). The layer surface potential decrease as a result of pulse illumination was up to 1–5% of the initial potential before illumination. The capacitance probe that was connected to the wide-frequency band electrometer measured the speed of the surface potential decrease (dU/dt). The transit time (t_t) was determined by the kink on the curve of the dU/dt transient on a linear or double logarithmic scale. The drift mobility was calculated by the formula $\mu = d^2/U_0 t_t$ (d is the layer thickness, U_0 is the surface potential at the moment of illumination).

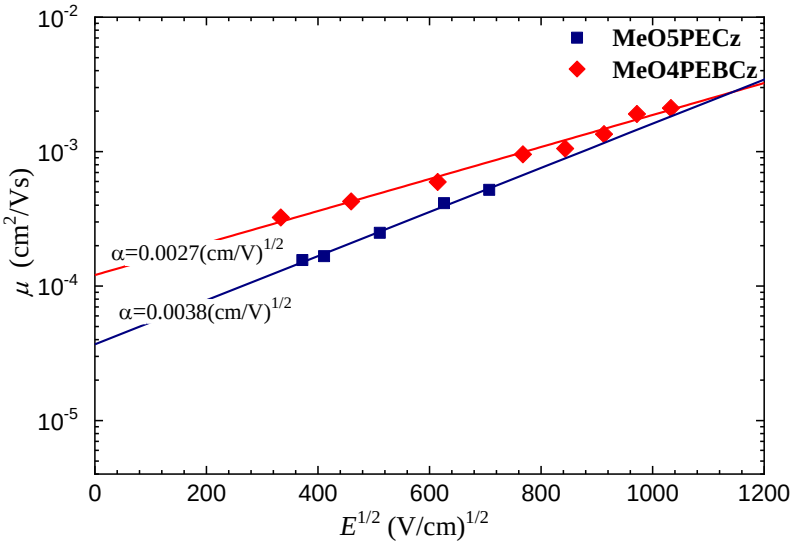

S 4. Drift carrier mobility of the tested HTMs

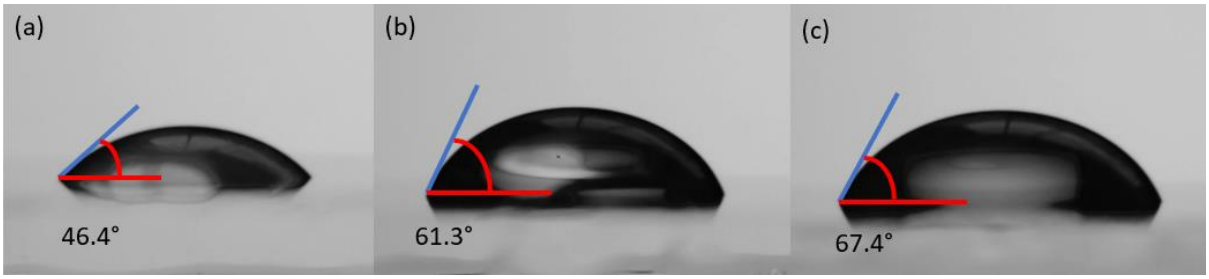

S 5. Water contact angle of films a) Spiro-OMeTAD doped with Li-TFSI and tBP b) MeO5PECz doped with tBP c) MeO4PEBCz doped with tBP

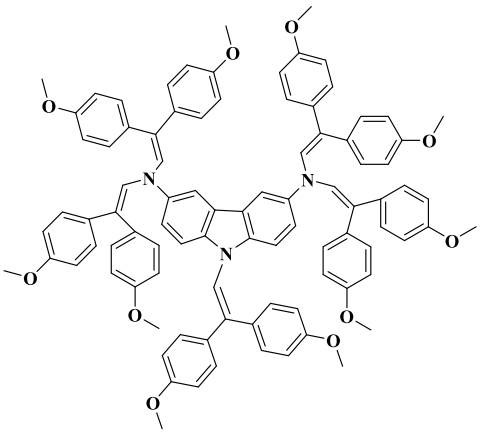

S 5. Molecular structure of N^3, N^3, N^6, N^6, 9-pentakis[2,2-bis(-methoxyphenyl)ethenyl]-9*H*-carbazole-3,6-diamine (MeO5PECz)

N^3, N^3, N^6, N^6, 9-pentakis[2,2-bis(-methoxyphenyl)ethenyl]-9*H*-carbazole-3,6-diamine (MeO5PECz): a mixture of 9*H*-carbazole-3,6-diamine (0.5 g, 2.5 mmol), 2,2-bis(4-methoxyphenyl)acetaldehyde (4.06 g, 15.8 mmol) and camphor-10-sulfonic acid (β) (0.59 g, 2.5 mmol) were dissolved in THF (10 ml + volume of the Dean-Stark trap ml), 3Å molecular sieves were added to absorb water. The mixture was heated under argon for 8 hours at reflux. Afterwards (TLC control 7:18 v/v acetone/*n*-hexane) the reaction mixture was cooled to room temperature and poured into 200 ml of ethanol. The precipitate was filtered and washed with 200 ml of ethanol and then crystalized from acetone giving MeO5PECz as yellow crystals (m. p. 187-189 °C). Yield: 2.05 g (58 %).

Elemental analysis calculated (%) for $C_{92}H_{81}N_3O_{10}$ (1388.67 g/mol): C 79.57; H 5.88; N 3.03. Found: C 79.31; H 6.01; N 3.16. MS (ESI); $[M+H^+]$ = 1389.

^{1}H NMR (700 MHz, $CDCl_3$) δ 7.69 (s, 2H), 7.38 (d, 8.7 Hz, 2H), 7.18 – 7.10 (m, 4H), 7.04 (dd, *J* = 28.6, 8.5 Hz, 10H), 6.97 – 6.88 (m, 2H), 6.86 – 6.75 (m, 8H), 6.70 – 6.55 (m, 11H), 6.46 (d, J = 8.5 Hz, 8H), 5.81 (s, 4H), 3.89 – 3.69 (m, 30H).

^{13}C NMR (176 MHz, $CDCl_3$) δ 159.78, 158.87, 158.85, 158.50, 136.58, 134.61, 133.63, 133.00, 131.14, 130.80, 130.66, 130.15, 129.94, 129.68, 128.81, 127.68, 124.24, 117.27, 114.39, 113.80, 113.74, 112.97, 110.98, 108.74, 55.40, 55.40, 55.19.

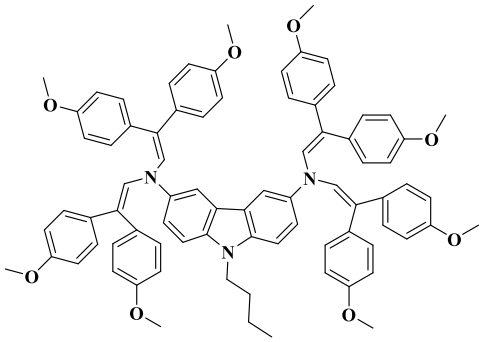

S 6. Molecular structure of N^3, N^3, N^6, N^6, 9-tetrakis[2,2-bis(-methoxyphenyl)ethenyl]-9-butyl-9*H*-carbazole-3,6-diamine (MeO4PEBCz)

N^3, N^3, N^6, N^6, 9-tetrakis[2,2-bis(-methoxyphenyl)ethenyl]-9-butyl-9*H*-carbazole-3,6-diamine (MeO4PEBCz): a mixture of 9-Butyl-9*H*-carbazole-3,6-diamine (1 g, 3.9 mmol), 2,2-bis(4-methoxyphenyl)acetaldehyde (5.0 g, 19.7 mmol) and camphor-10-sulfonic acid (β) (0.9 g, 3.9 mmol) were dissolved in toluene (10 ml + volume of the Dean-Stark trap ml). The mixture was heated for 1 hour at reflux. Afterwards (TLC control 5:20 v/v acetone/*n*-hexane) the reaction mixture was cooled to room temperature and extracted with ethyl acetate. The organic layer was dried over anhydrous Na_2SO_4, filtered, the solvent was removed. The crude product was washed with hot ethanol giving green crystals, which then were recrystallized from a mixture of THF and ethanol (1:1) giving MeO4PEBCz as yellowish crystals (247-249 °C). Yield: 2.31 g (49 %).

Elemental analysis calculated (%) for $C_{80}H_{75}N_3O_8$ (1206.49 g/mol): C 79.64; H 6.27; N 3.48. Found: C 79.41; H 6.39; N 3.59. MS (ESI); $[M+H^+]$ = 1207

^{1}H NMR (400 MHz, $CDCl_3$) δ 7.72 (d, J = 8.8 Hz, 2H), 7.38 – 7.11 (m, 4H), 7.09 – 6.91 (m, 10H), 6.86 – 6.67 (m, 10H), 6.62 – 6.30 (m, 14H), 5.79 (s, 2H), 3.79 – 3.58 (m, 24H), 1.77 (d, J = 3.0 Hz, 4H), 1.33 (td, J = 15.1, 7.6 Hz, 2H), 0.88 (t, J = 7.2 Hz, 3H).

^{13}C NMR (101 MHz, $CDCl_3$) δ 159.01, 158.95, 158.86, 158.84, 130.65, 130.18, 128.81, 128.51, 114.42, 113.81, 113.16, 113.04, 113.00, 112.86, 68.00, 55.42, 55.31, 55.26, 55.22, 25.63, 20.60, 13.96.

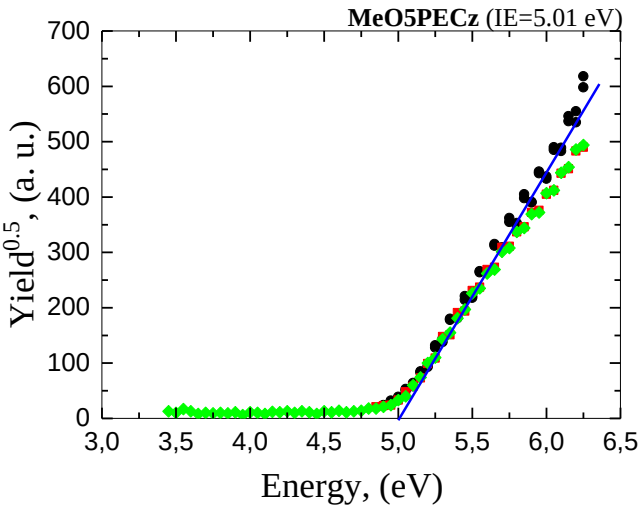

S 7. *Ip* measurements of MeO5PECz

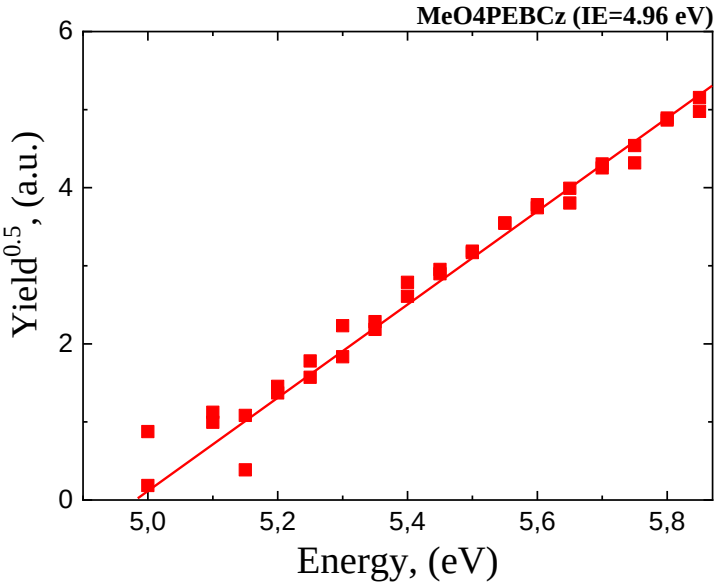

S 8. *Ip* measurement of MeO4PEBCz

a)

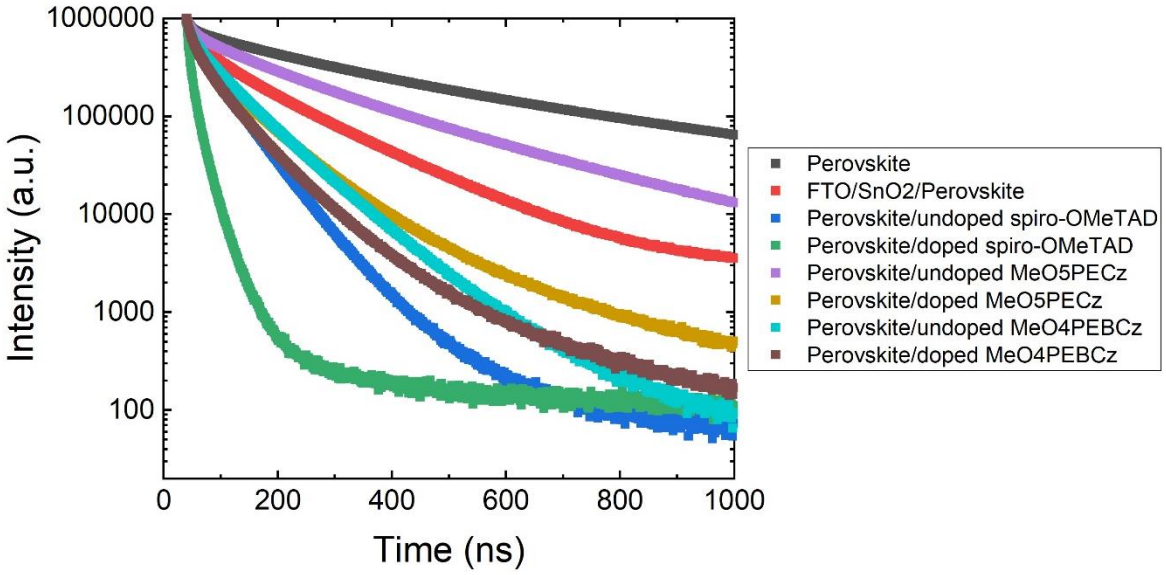

b)

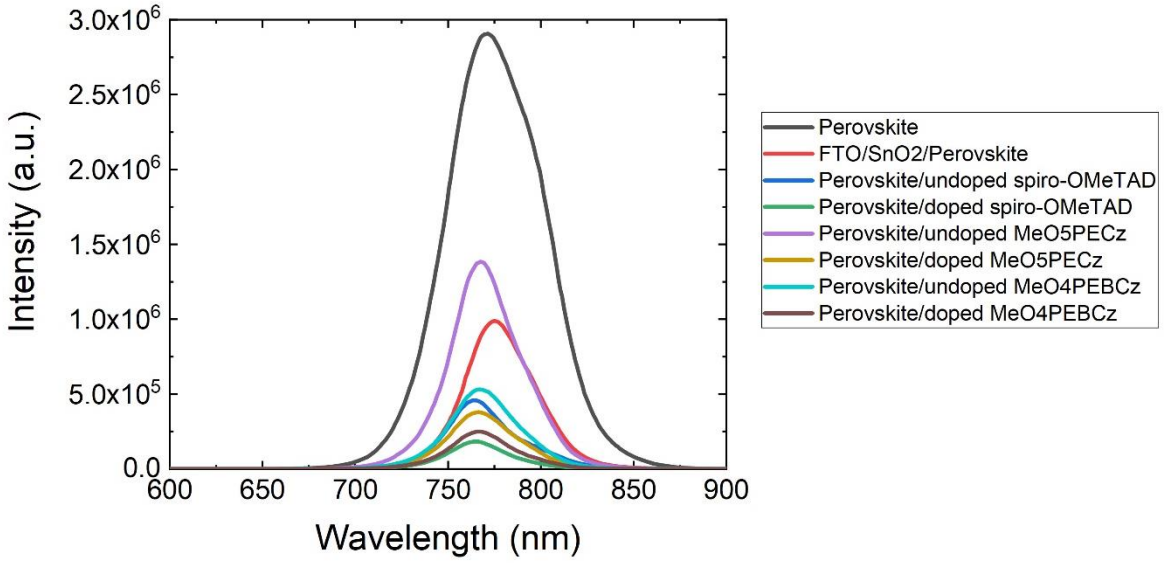

S 10. a) Time-resolved photoluminescence measurements of perovskite films on glass (pristine), perovskite coated with spiro-OMeTAD doped with both *t*BP and Li-TFSI, and perovskite with the new enamine hole-transporting materials with and without both Li-TFSI and tBP dopants. b) Their corresponding steady-state photoluminescence

Table S2. TRPL curve fitted parameters according to equation 1 and equation 2.

	τ (ns)	β	Lifetime (ns)
Perovskite	244.4	0.70	308.4
Perovskite/Spiro (neat)	34.6	0.77	40.2

Perovskite/Spiro (50%mol Li-TFSI, tBP)	6.7	0.74	8.1
Perovskite/MeO5PECz (neat)	126.2	0.70	160.3
Perovskite/MeO5PECz (25%mol Li-TFSI, tBP)	37.0	0.67	48.9
Perovskite/MeO4PEBCz (neat)	41.0	0.70	52.0
Perovskite/MeO4PEBCz (25% mol Li-TFSI, tBP)	28.2	0.68	36.9
FTO/SnO_2/Perovskite	60.8	0.62	87.3

Table S3. Photoluminescence properties and estimated quasi-Fermi level splitting (QFSL) of $FA_{0.83}Cs_{0.17}Pb(I_{0.9}Br_{0.1})_3$ perovskite thin-films coated on glass substrates and coated with different HTMs, with and without Li-TFSI doping. All samples were illuminated from the glass side similar to in devices. The data reported in the table were averaged across four PLQE measurements for each condition. The errors given for the PLQE are the statistical error of the measurements, and those for the QFLS are the propagated errors from the PLQE. The excitation wavelength for the TRPL was 510 nm. For the PLQE measurements and subsequent QFLS calculations, the excitation was measured using a 532 nm laser, with an absorbed photon fluence approximately matching AM1.5 100mW/cm^{-2} irradiance. Dopant concentration in each type of HTM is optimized for best device performance.

Half-stack			
HTM	**TRPL Mean Lifetime (ns)**	**PLQE (%)**	**QFLS (eV)**
Perovskite	308.4	6.6±0.5	1.249±0.002
Perovskite/Spiro (neat)	40.2	0.32±0.05	1.171±0.004
Perovskite/Spiro (50%mol Li-TFSI, tBP)	8.1	0.2±0.1	1.15±0.02
Perovskite/MeO5PECz (neat)	160.3	4.8±0.8	1.241±0.004
Perovskite/MeO5PECz (25%mol Li-TFSI, tBP)	48.9	0.9±0.2	1.196±0.006
Perovskite/MeO4PEBCz (neat)	52.0	1.0±0.3	1.201±0.006

Perovskite/MeO4PEBCz (25% mol Li-TFSI, tBP)	36.9	0.53±0.04	1.184±0.002
FTO/SnO_2/Perovskite	87.3	0.36±0.07	1.174±0.005

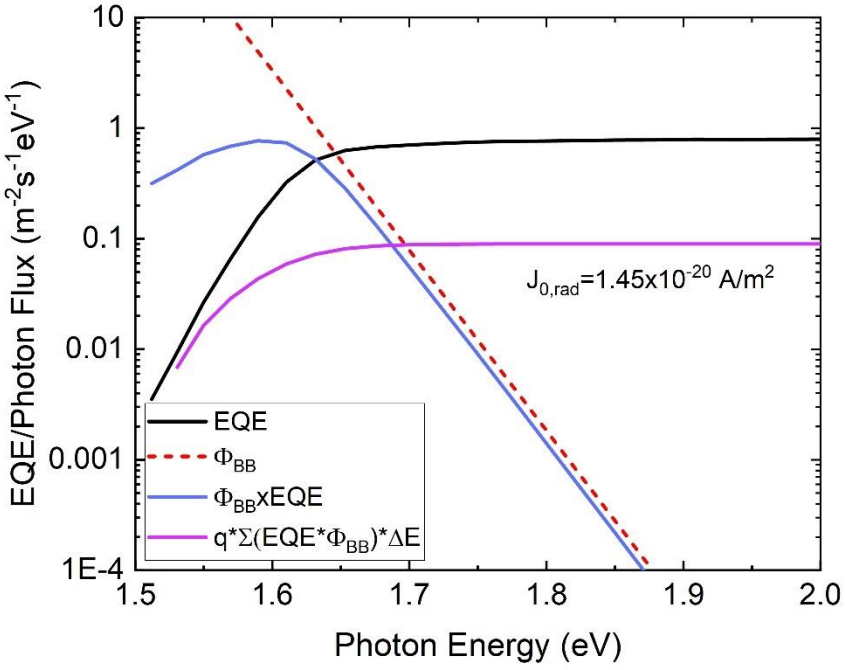

S11. EQE_{PV} onset (black line) convoluted with the black-body (Φ_{BB}) radiation of the surroundings at 300K (red dotted line). The perovskite emission spectra resulted from the convolution is plotted in blue. The emission spectra is integrated over the photon energy and multiplied by the elementary charge q in order to calculate the dark radiative current $J_{0,rad}$, plotted in purple.

The approach used follows that reported by Rau et al.[4] Briefly, the black body photon flux is

$$\phi_{BB} = \frac{1}{4\pi^2\hbar^3c^2}\frac{E^2}{\exp\left(\frac{E}{k_BT}\right)-1} \qquad \text{Equation (S3).}$$

Where $\hbar$ is the reduced Planks constant, k_B is the Boltzmann constant and T is the temperature. Assuming that the perovskite solar cell is at 300K in thermal equilibrium with its environment, the dark radiative recombination current is

$$J_{em,0} = q\int EQE_{PV}(E)\phi_{BB}(E)dE = J_{rad,0} \qquad \text{Equation (S4).}$$

With EQE_{PV} the photovoltaic external quantum efficiency of the perovskite solar cell and $J_{em,0}$ the current giving rise to emission, which also defines the dark radiative recombination current at V=0. From that, the radiative limit of the QFLS ($QFLS_{rad}$) at EQE_{EL}=1 can be calculated with the following equation

$$QFLS_{rad} = \frac{k_BT}{q}\ln\left(\frac{J_G}{J_{rad,0}}\cdot 1\right) \qquad \text{Equation (S5).}$$

Where J_G is the generation current under illumination, in this case approximated to the short circuit current J_{sc}.

We calculated the radiative V_{oc} of our perovskite absorber by using equation S5.

$$V_{OC,rad} = \frac{k_B T}{q} \ln\left(\frac{J_{SC}}{J_{0,rad}}\right) = 1.320\ V \qquad \text{Equation (S6).}$$

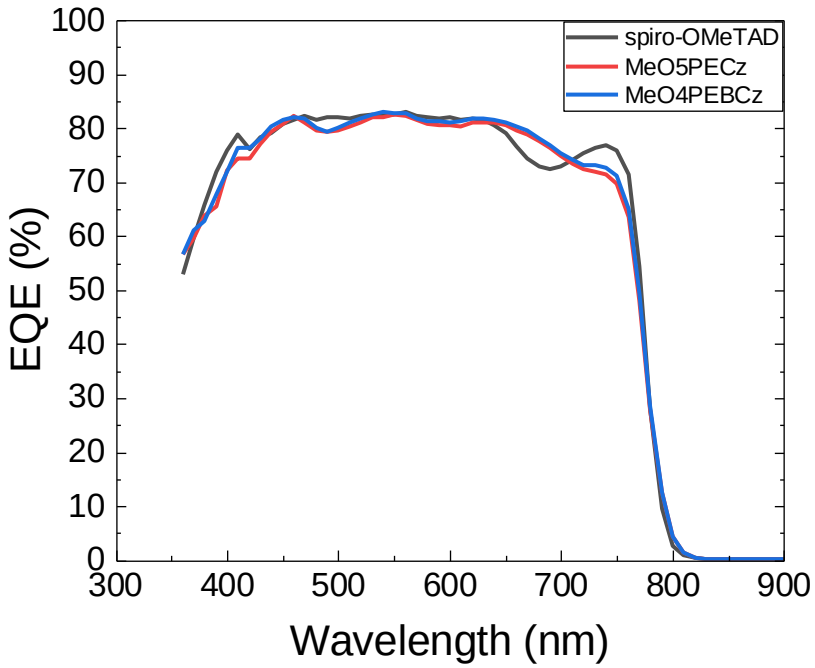

S12. External quantum efficiency of devices with spiro-OMeTAD (doped with tBP and Li-TFSI), undoped MeO5PECz and undoped MeO4PEBCz as HTMs.

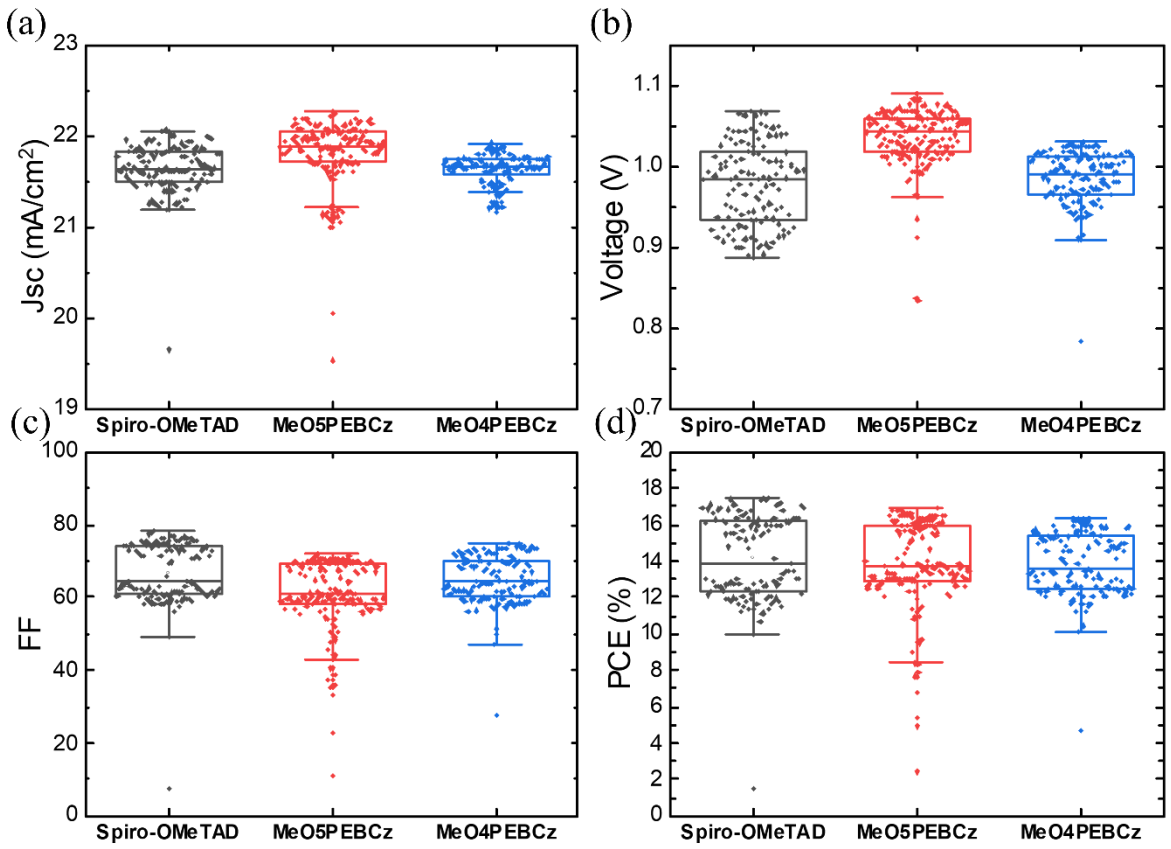

S13. Box plots of device a) short-circuit current, b) open-circuit voltage, c) fill factor and d) power conversion efficiencies. Spiro-OMeTAD was doped with both tBP and Li-TFSI, while the carbazole-based HTMs were dopant-free.

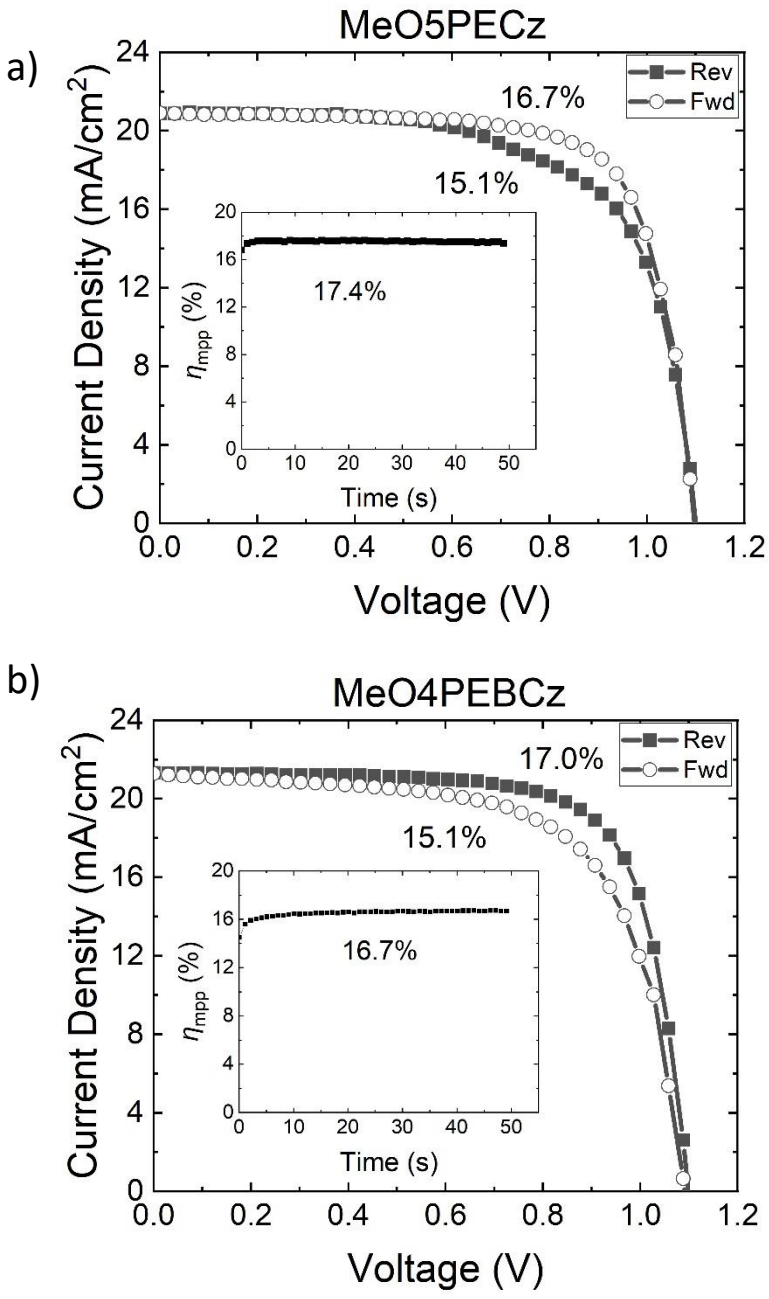

Figure S14. a) J-V scan of MeO5PECz device. MeO5PECz was doped with both Li-TFSI and tBP b) J-V scans of MeO4PEBCz device. MeO4PEBCz was doped with both Li-TFSI and tBP. The insets shows their maximum power point tracked efficiencies for 50 seconds.

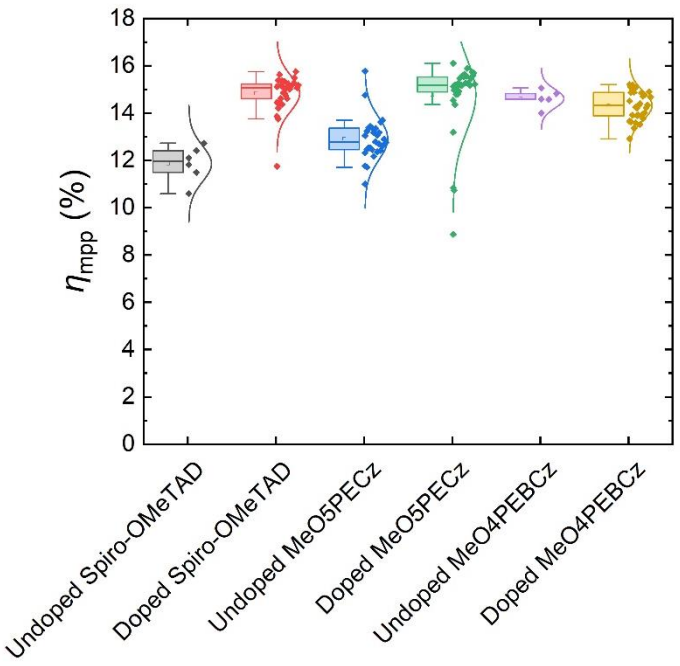

Figure S15. Maximum power point tracked efficiencies (η_{mpp}) (for 33 seconds) comparison between undoped HTMs and their corresponding counterparts doped with both Li-TFSI and tBP. Spiro-OMeTAD was doped with 50 mol% Li-TFSI and 33 µL/mL tBP. Both MeO5PECz and MeO4PEBCz were doped with 25 mol% Li-TFSI and 33 µL/mL tBP which were optimized for best device performances.

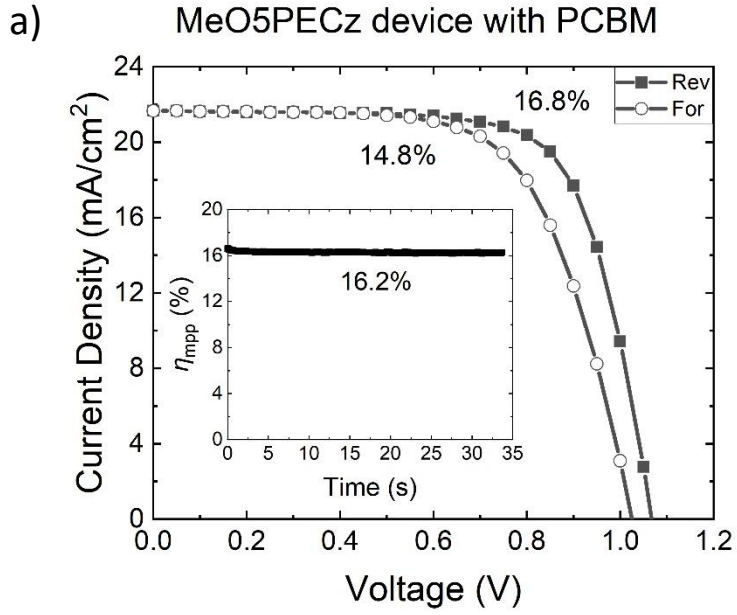

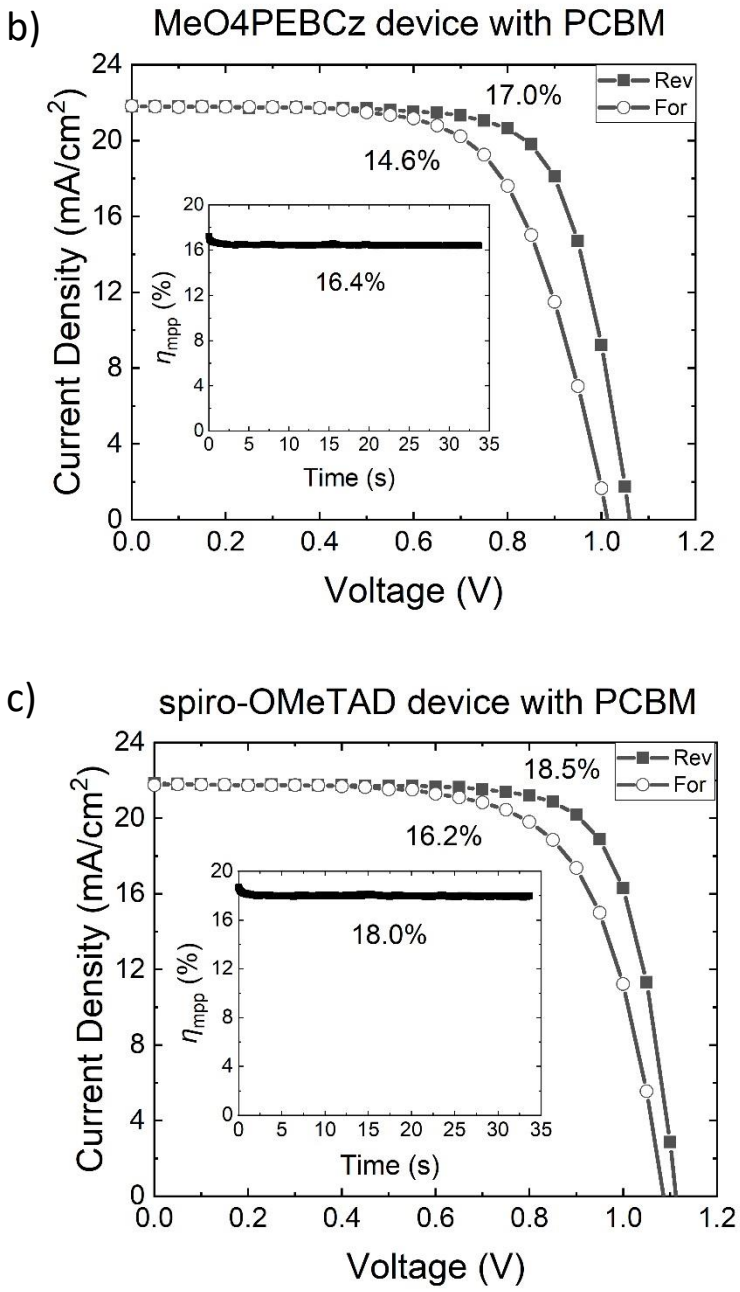

Figure S16. J-V curves of a) undoped MeO5PECz b) undoped MeO4PEBCz and c) doped spiro-OMeTAD devices each with an extra PCBM layer in between the SnO_2 and perovskite. The insets show the stabilized maximum power point efficiencies.

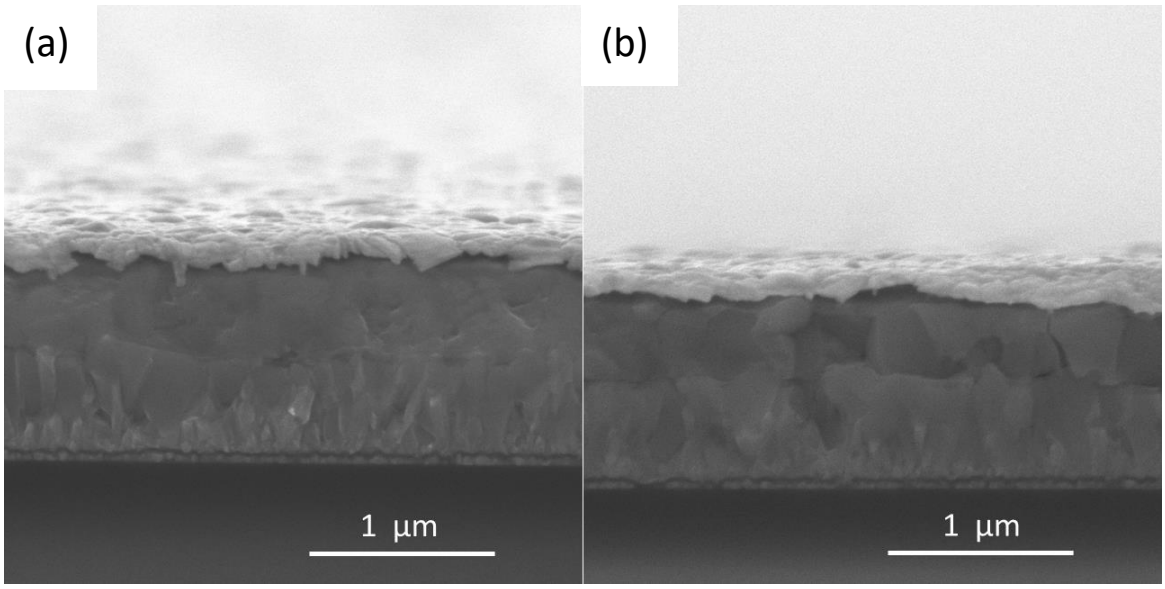

Figure S17. Cross-sectional SEM image of devices with a) Undoped MeO5PECz and b) Undoped MeO4PEBCz as HTMs.

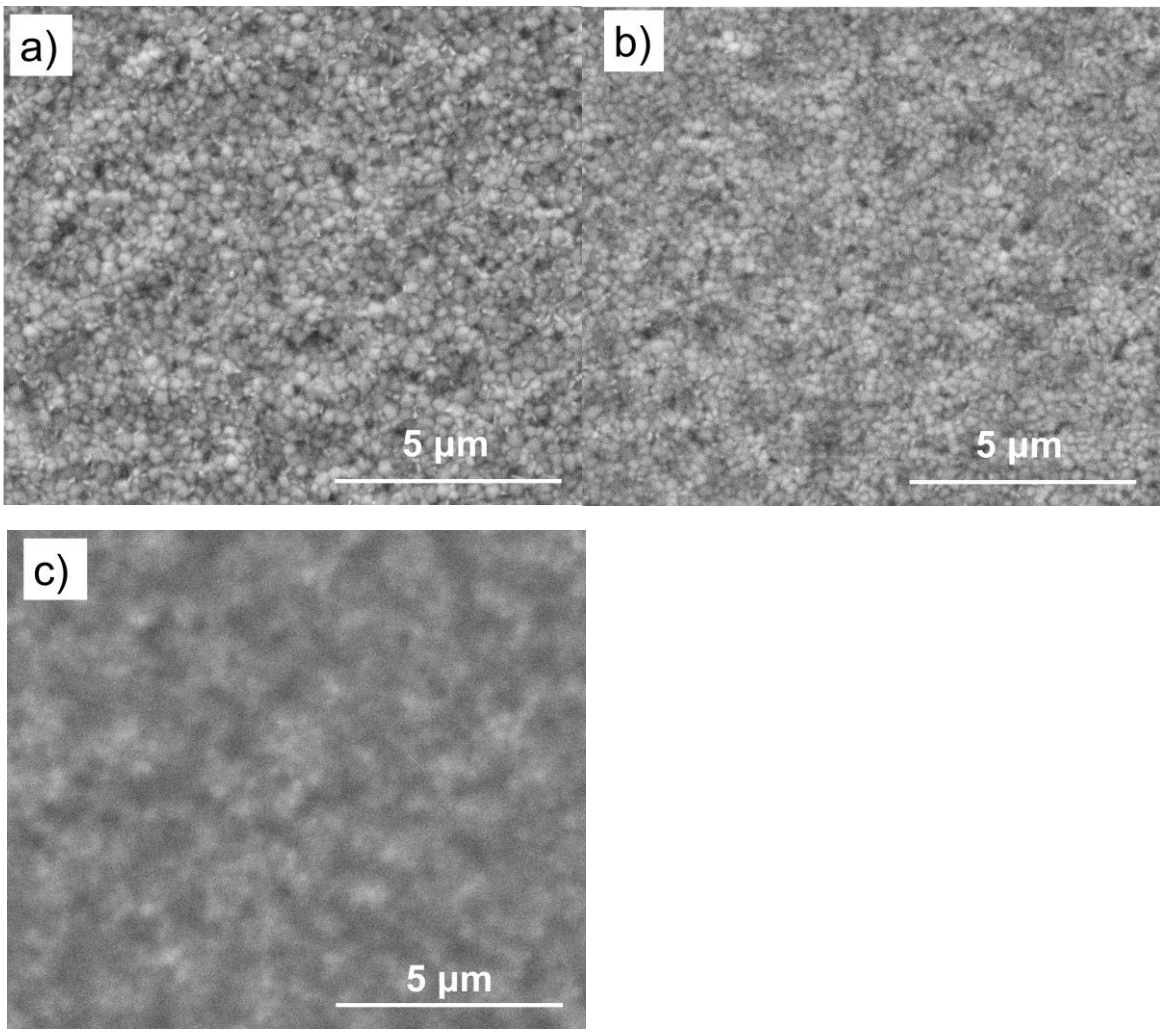

Figure S18. SEM images of a) undoped MeO5PECz b) undoped MeO4PEBCz and c) doped spiro-OMeTAD on top of perovskite.

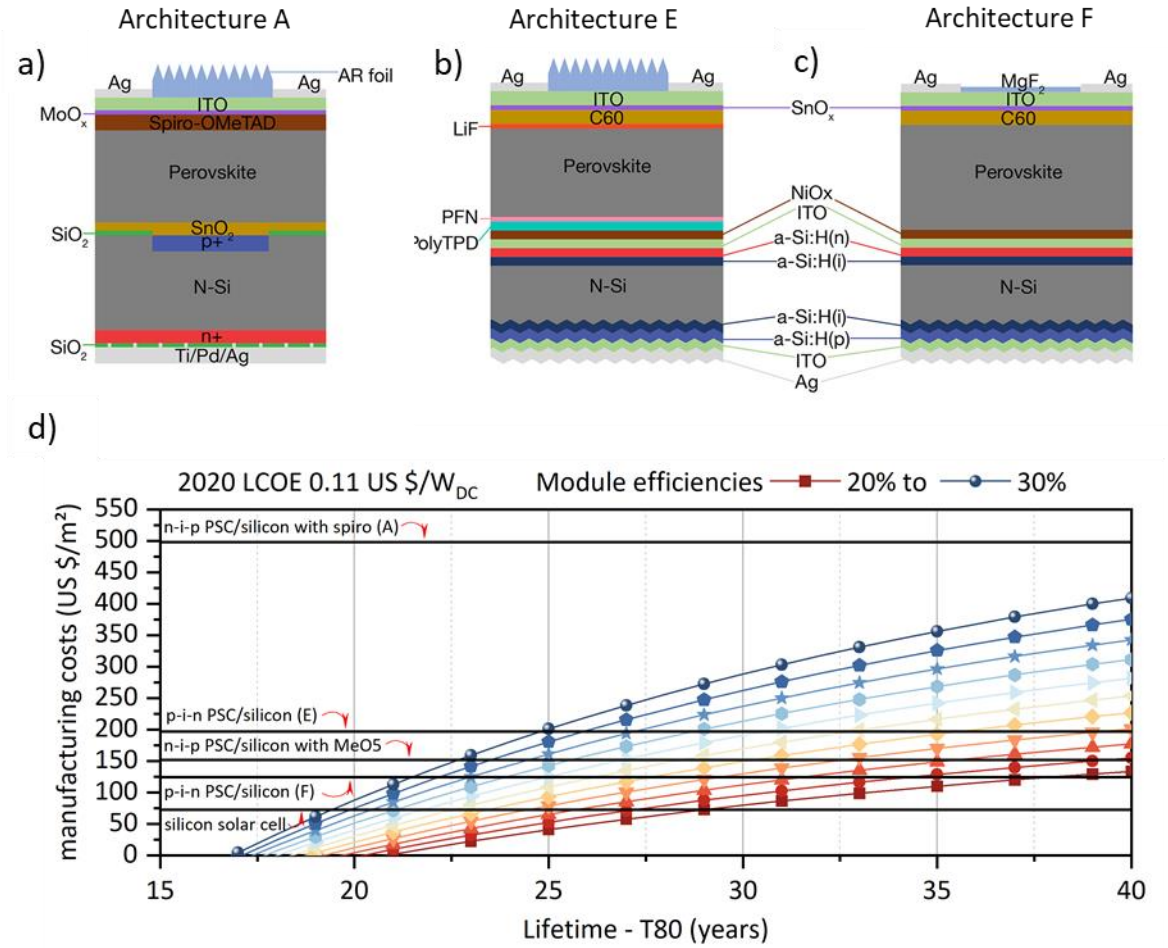

Figure S19. Published manufacturing cost for silicon/perovskite tandems architectures. a) to c) are reprinted from (ref.[6]) with permission from John Wiley and Sons. a) Architecture A reaching 17.1% PCE on a 16-cm^2 area.[7] b) Architecture E reaching 27% PCE on 1-cm^2.[8] c) Architecture F reaches 22.6% on an area of 57.4 cm^2.[9] d) The calculated manufacturing costs as function of module efficiencies and lifetimes.

Cost estimation

Diamine carbazole precursors could be obtained commercially or synthesized *via* two or three step procedure (Figure S 20) according to the procedures reported in the literature [10,11,12]. Due to low volumes of production and niche application of the commercial diamine products its price is rather high, therefore, at the moment, for larger scale synthesis, it makes more economic

sense to synthesize the precursors inhouse. Therefore, we have included cost of precursor synthesis into the cost estimation calculations.

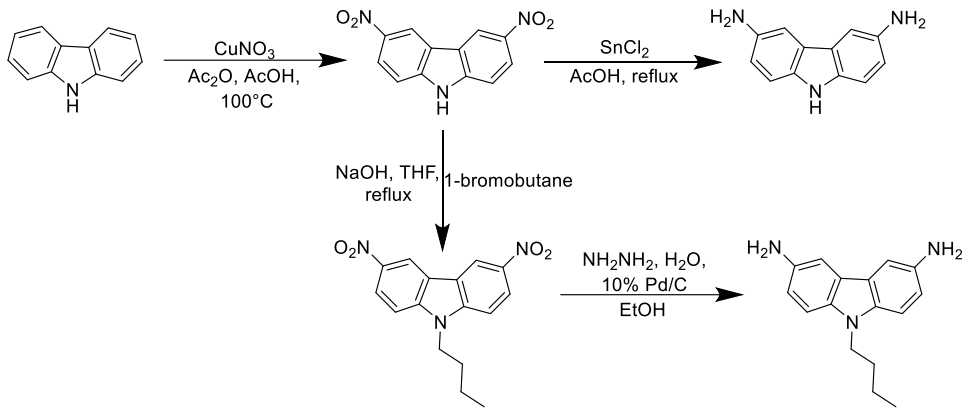

Figure S 20. Synthesis of carbazole precursors.

Materials intended for use on a large scale must be not only efficient but also cost-effective. For that reason, the estimation of the synthesis costs for both carbazole derivatives has been done based on the procedure established by Osedach et al. (Table S4, S5).[13] It was calculated that the synthesis cost of MeO5PECz is $ 7.83 per gram while for MeO4PEBCz it reaches 10.33 $/g. It would cost 10 to 12 times less to produce these HTMs than widely used standard spiro-OMeTAD, which costs $ 92 per gram to synthesize.[14] Synthesis of MeO5PECz and MeO4PEBCz does not require expensive column chromatography or sublimation, the purification is done by simple crystallization; furthermore, the palladium-catalyzed cross-coupling is not needed, avoiding traces of catalyst residue in the final step, which might act as photoquenchers or charge traps during device operation.[15,16]

Table S4. Materials, quantities, and cost for the synthesis of MeO5PECz.

Chemicals	Weight reagent (g/g)	Weight solvent (g/g)	Weight Workup (g/g)	Price of chemicals (€/kg)	Cost of chemical (€/g product)	Cost per step (€/g)
Carbazole	0.28			200.00	0.05	
$Cu(NO_3)_2$	0.49			23.12	0.01	
Acetic acid		2		40.12	0.08	

Acetic anhydride		2.5		12.00	0.03	
Ethanol			30	6.08	0.20	
KOH			2.5	12.70	0.03	
HCl			10	4.31	0.04	
3,6-dinitro-9*H*-carbazole	**0.77**	**4.5**	**42.5**			**0.44**
$SnCl_2$	2.63			118.10	0.31	
Acetic acid		2.5		40.12	0.10	
HCl		12		4.31	0.05	
NaOH			20	4.28	0.09	
3,6-diamino-9*H*-carbazole	**2.63**	**14.5**	**20**			**0.55**
2,2-bis(4-methoxyphenyl)acetaldehyde	2.03			2300.00	4.67	
CSA	0.3			260.00	0.08	
THF		15		8.88	0.13	
Ethanol			200	6.08	1.22	
Acetone			22	1.52	0.04	
Total	**5.73**	**34**	**284.5**			**7.13**

7.13€=7.83$

Table S5. Materials, quantities and cost for the synthesis of MeO4PEBCz.

Chemicals	Weight reagent (g/g)	Weight solvent (g/g)	Weight Workup (g/g)	Price of chemicals (€/kg)	Cost of chemical (€/g product)	Cost per step (€/g)
3,6-dinitro-9*H*-carbazole	0.85			1222.22	1.04	
1-bromobutane	0.906			22.08	0.02	
THF		125	15	8.88	1.24	
NaOH	0.27			4.28	0.01	
9-butyl-3,6-dinitrocarbazole	**2.026**	**125**	**15**			**2.31**
Pd/C	0.05			5350.00	0.27	

$N_2H_4 \cdot xH_2O$	1			22.00	0.02	
Ethanol		17	4	6.08	0.13	
9-alkyl-3,6-diaminocarbazole	**1.05**	**17**	**4**			**0.42**
2,2-bis(4-methoxyphenyl)acetaldehyde	2.2			2300.00	5.06	
CSA	0.4			260.00	0.10	
Toluene		15		2.46	0.04	
Ethyl acetate			125	2.85	0.35	
Na_2SO_4			20	6.08	0.12	
Ethanol			100	6.08	0.61	
THF			45	8.88	0.4	
Total	**5.676**	**157**	**309**			**9.41**

9.41€=10.33$

Supplementary Note 1. Cost Analysis

Below is the complete used formula for the LCOE calculations. We assume a loan and a MACRS depreciation system similar to the US Solar Photovoltaic System and Energy Storage Cost Benchmark: Q1 2020.[14]

$$LCOE = \frac{(Man + BoS)(1 - debt_{frac}) + \sum_{t=1}^{n=30} \frac{O\&M_t - Tax_{\ eff.}\left(Depr_t + O\&M_t + Debt_{prin,t}\right) + (Man + BoS)\ debt_{frac}(debt_{nom,t} + debt_{prin,t})}{(1 + \delta_{nom})^t}}{\sum_{t=1}^{n=30} \frac{Yield_t(1 - Tax_{\ eff.})}{(1 + \delta_{real})^t}}$$

With Man = Manufacturing cost; BoS = Balance of System cost; $debt_{frac}$ = debt fraction; O&M = Operation and Maintenance cost; Tax_{eff} = the effective tax rate; $Debt_{prin}$= principle payment of the debt; $debt_{nom,t}$ = nominal debt fraction coefficient; $debt_{prin,t}$ = principle debt coefficient; δ_{nom} = nominal discount rate; δ_{real} = real discount rate; $Yield_t$ = produced energy of the system in year t calculated by SAM for Phoenix, Nevada (USA). We take the average US efficiency of 19.5%, a lifetime (LT) of 30 years and a system size of 7 kW_{DC}. The exact input parameters are outlined below. For the Man_0(LT, PCE) we reformulate the above-outlined LCOE formula to:

$$Man_0(LT, PCE) = \left(LCOE * \sum_{t=1}^{n=LT} \frac{Yield(LT)(1 - Tax_{eff})}{(1 + \delta_{real})^t} - BoS_0(PCE)\left(1 - debt_{frac}\right) - \sum_{t=1}^{n=LT} \frac{O\&M_t\left(1 - Tax_{eff}\right)}{(1 + \delta_{nom})^t} \right.$$

$$\left. - \sum_{t=1}^{n=18} \frac{BoS_0(PCE) * debt_{frac}(debt_{nom,t} + debt_{prin,t}(1 - Tax_{eff}))}{(1 + \delta_{nom})^t} - \sum_{t=1}^{n=6} \frac{BoS_0(PCE) * Tax_{eff} * a_t}{(1 + \delta_{nom})^t} \right)$$

$$/\left(1 - debt_{frac} + \sum_{t=1}^{n=18} \frac{debt_{frac}(debt_{nom,t} + debt_{prin,t}(1 - Tax_{eff}))}{(1 + \delta_{nom})^t} - \sum_{t=1}^{n=6} \frac{Tax_{eff} * a_t}{(1 + \delta_{nom})^t} \right)$$

The Yield(LT) is given by assuming a linear decay in each year until the end of the module lifetime at 80% of its initial efficiency (T80). For example, if the module would have a lifetime of 2 years it would produce each year 10% less energy which can be expressed as shown below. So, for the energy yield calculation we derived the following equation:

$$Yield\ (LT) = 0.9 * LT * Yield_0$$

Were LT is given in years and $Yield_0$ is the initial energy production in the first year assuming no degradation. We note that we assume that a perovskite solar module system would produce as much energy as silicon solar module system of the same size and efficiency. The factors a_t are given by the Modified Accelerated Cost Recovery System (MACRS) in the U.S. which is the typical tax depreciation. They are as follows:

$$a_t = \{0.2, 0.32, 0.192, 0.1152, 0.1152, 0.0576\}$$

For the efficiency dependence of the model, we assumed that the total system size would stay equal. Thus, lower efficiency of the modules would be compensated by a larger used area. A higher efficient module would need less area. Accordingly, all cost related to the area changed equally. Those are here the module cost and parts of the BoS which are the overhead, the supply chain costs, the sales tax, the installation labour and the structural BoS. Further assumptions are outlined below.

Table S6. Input parameters based on the US Solar Photovoltaic System and Energy Storage Cost Benchmark: Q1 2020 report[14], calculations were done for a 19.5% PCE efficient Si module with a lifetime of 30 years in Phoenix, Nevada (USA)

Residential System in kW_{DC}	**7**	**Inverter efficiency**	**98%**
Inflation rate	2.5%	**Inverter Lifetime**	20
Real discount rate	6.1%	**Degradation**	0.7%
Nominal discount rate	8.75%	**Federal Tax rate**	21%
Debt Fraction	53.7%	**State Tax**	6%
Nominal debt	4%	**Effective Tax Rate**	0.2574
WACC	5.65%	**O&M costs ($/kW/yr)**	29.00

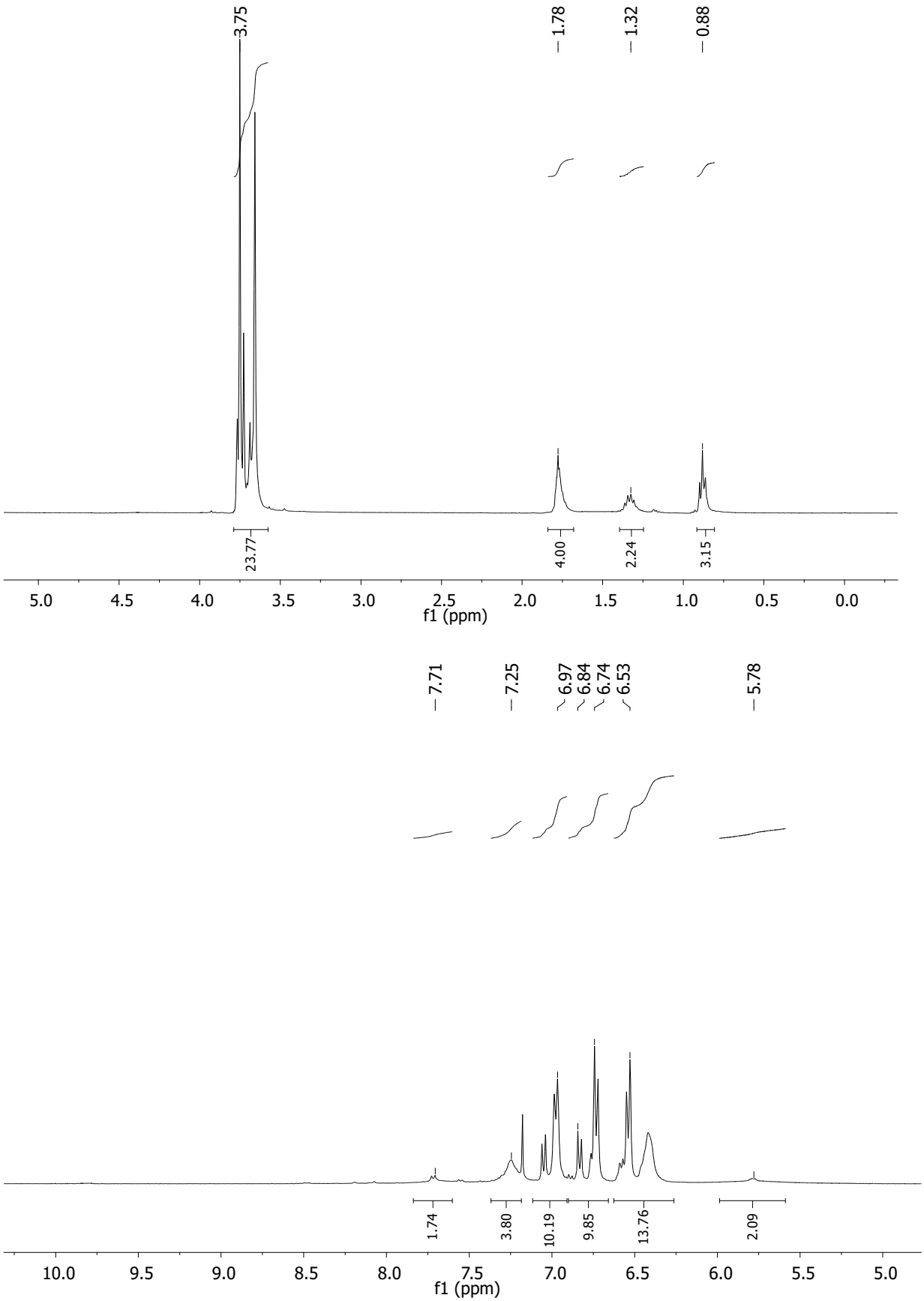

Figure S 21. N^3, N^3, N^6, N^6, 9-tetrakis[2,2-bis(-methoxyphenyl)ethenyl]-9-butyl-9*H*-carbazole-3,6-diamine (MeO4PEBCz). ^{1}H NMR (400 MHz, $CDCl_3$, δ, ppm).

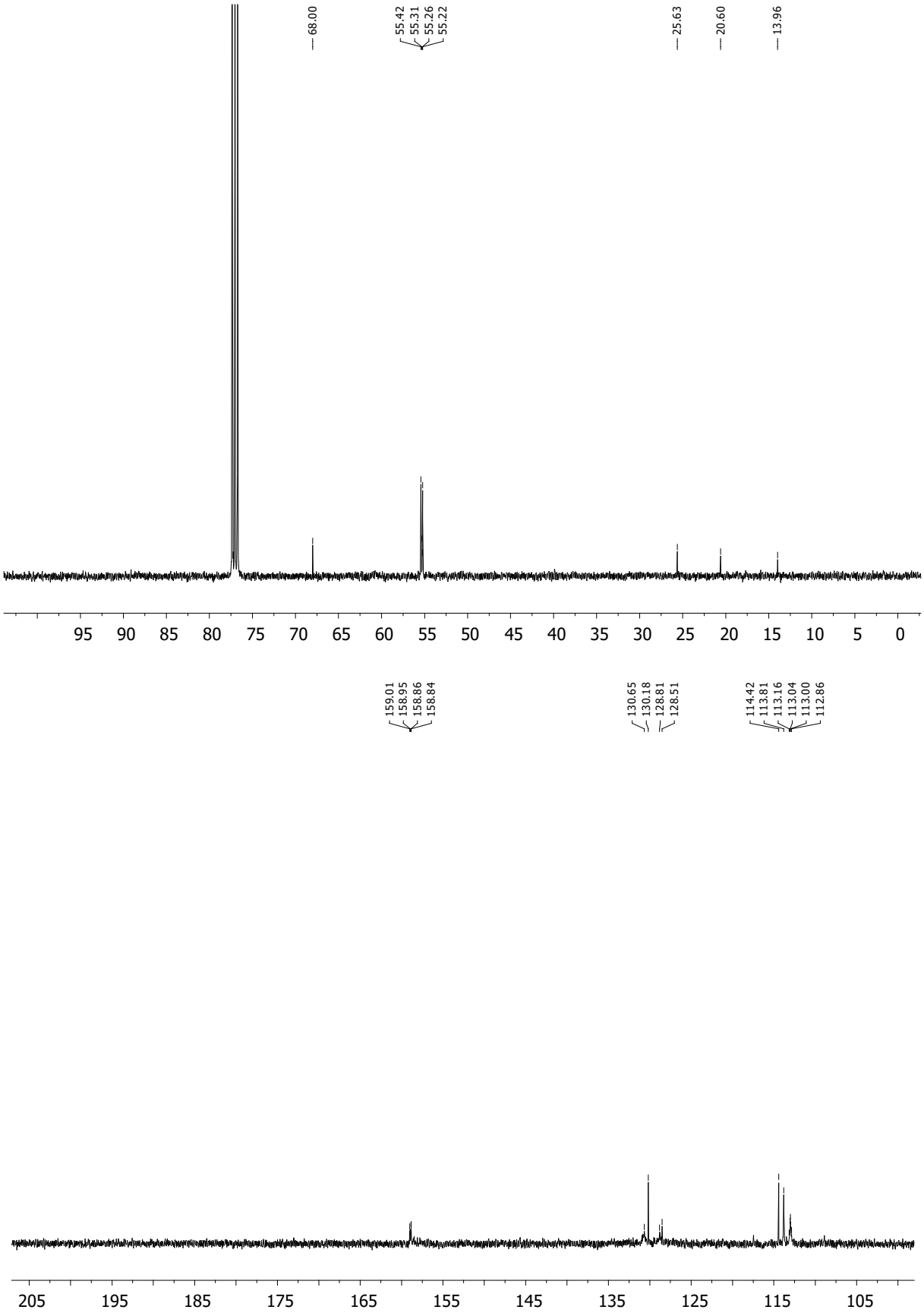

Figure S 22. *N*^{3}, *N*^{3}, *N*^{6}, *N*^{6}, 9-tetrakis[2,2-bis(-methoxyphenyl)ethenyl]-9-butyl-9*H*-carbazole-3,6-diamine (MeO4PEBCz). ^{13}C NMR (101 MHz, $CDCl_3$, δ, ppm).

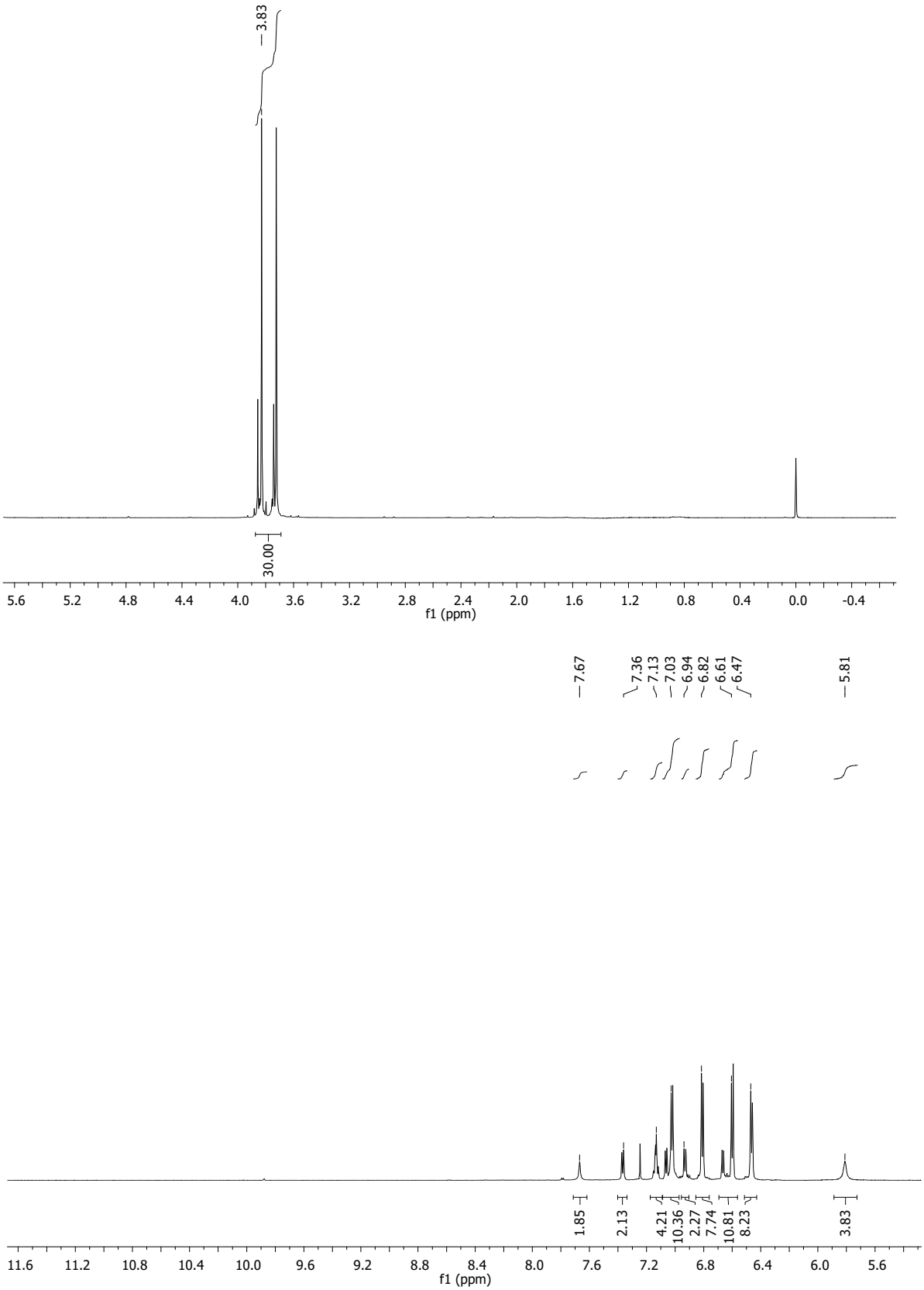

Figure S 23. N^3, N^3, N^6, N^6, 9-pentakis[2,2-bis(-methoxyphenyl)ethenyl]-*9H*-carbazole-3,6-diamine (MeO5PECz). ^{1}H NMR (700 MHz, $CDCl_3$, δ, ppm).

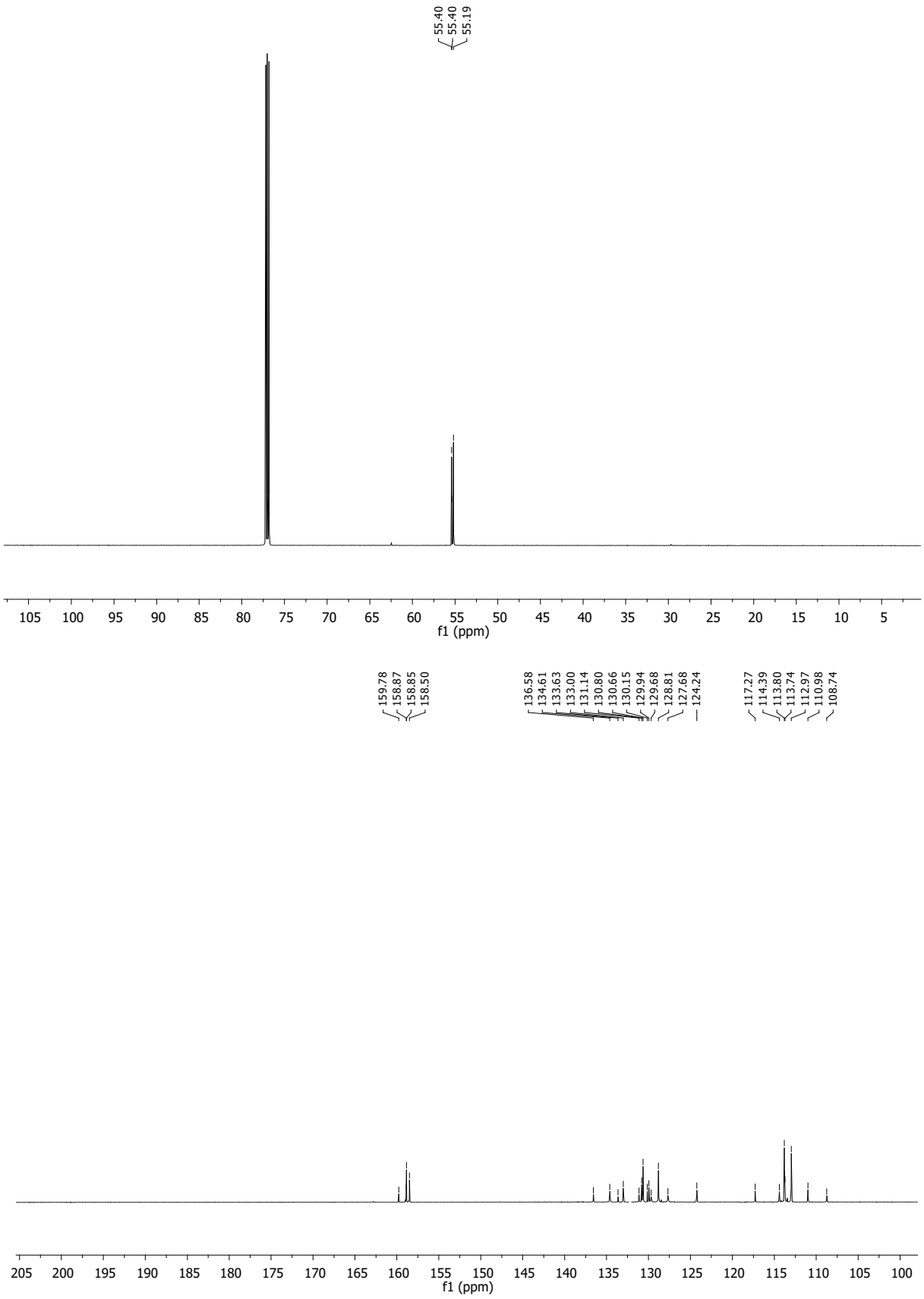

Figure S 24. *N*^{3}, *N*^{3}, *N*^{6}, *N*^{6}, 9-pentakis[2,2-bis(-methoxyphenyl)ethenyl]-*9H*-carbazole-3,6-diamine (MeO5PECz). ^{1}H NMR (176 MHz, $CDCl_3$, δ, ppm).

References

[1] S. N. Habisreutinger, B. Wenger, H. J. Snaith, R. J. Nicholas, *ACS Energy Lett.* **2017**, *2*, 622.

[2] J. C. de Mello, H. F. Wittmann, R. H. Friend, *Adv. Mater.* **1997**, *9*, 230.

[3] P. Caprioglio, M. Stolterfoht, C. M. Wolff, T. Unold, B. Rech, S. Albrecht, D. Neher, *Adv. Energy Mater.* **2019**, *9*, 1901631.

[4] U. Rau, *Phys. Rev. B* **2007**, *76*, 085303.

[5] T. Kirchartz, J. A. Márquez, M. Stolterfoht, T. Unold, *Adv. Energy Mater.* **2020**, *10*, 1904134.

[6] N. L. Chang, J. Zheng, Y. Wu, H. Shen, F. Qi, K. Catchpole, A. Ho-Baillie, R. J. Egan, *Prog. Photovoltaics Res. Appl.* **2021**, *29*, 401.

[7] J. Zheng, C. F. J. Lau, H. Mehrvarz, F.-J. Ma, Y. Jiang, X. Deng, A. Soeriyadi, J. Kim, M. Zhang, L. Hu, X. Cui, D. S. Lee, J. Bing, Y. Cho, C. Chen, M. A. Green, S. Huang, A. W. Y. Ho-Baillie, *Energy Environ. Sci.* **2018**, *11*, 2432.

[8] J. Xu, C. C. Boyd, Z. J. Yu, A. F. Palmstrom, D. J. Witter, B. W. Larson, R. M. France, J. Werner, S. P. Harvey, E. J. Wolf, W. Weigand, S. Manzoor, M. F. A. M. Van Hest, J. J. Berry, J. M. Luther, Z. C. Holman, M. D. McGehee, *Science (80-.).* **2020**, DOI 10.1126/science.aaz4639.

[9] B. A. Kamino, B. Paviet-Salomon, S.-J. Moon, N. Badel, J. Levrat, G. Christmann, A. Walter, A. Faes, L. Ding, J. J. Diaz Leon, A. Paracchino, M. Despeisse, C. Ballif, S. Nicolay, *ACS Appl. Energy Mater.* **2019**, *2*, 3815.

[10] T. P. Osedach, T. L. Andrew, V. Bulović, *Energy Environ. Sci.* **2013**, DOI 10.1039/c3ee24138f.

[11] M. L. Petrus, T. Bein, T. J. Dingemans, P. Docampo, *J. Mater. Chem. A* **2015**, DOI 10.1039/c5ta03046c.

[12] M. Degbia, M. Ben Manaa, B. Schmaltz, N. Berton, J. Bouclé, R. Antony, F. Tran Van, *Mater. Sci. Semicond. Process.* **2016**, *43*, 90.

[13] Ö. Usluer, M. Abbas, G. Wantz, L. Vignau, L. Hirsch, E. Grana, C. Brochon, E. Cloutet, G. Hadziioannou, *ACS Macro Lett.* **2014**, *3*, 1134.

[14] D. Feldman, V. Ramasamy, R. Fu, A. Ramdas, J. Desai, R. Margolis, *U.S. Solar Photovoltaic System and Energy Storage Cost Benchmark: Q1 2020*, United States, **2021**.